LA-2061
Copy No. C.3

AEC RESEARCH AND DEVELOPMENT REPORT

LOS ALAMOS SCIENTIFIC LABORATORY
OF THE UNIVERSITY OF CALIFORNIA ○ LOS ALAMOS NEW MEXICO

SCATTERING OF FAST NEUTRONS BY U^{238}

[redacted]

Printed in USA. Charge 35 cents. Available from the U. S. Atomic Energy Commission, Technical Information Service Extension, P. O. Box 1001, Oak Ridge, Tennessee. Please direct to the same address inquiries covering the procurement of other classified AEC reports.

APPROVED FOR PUBLIC RELEASE

[redacted] UNCLASSIFIED

LA-2061
PHYSICS AND MATHEMATICS

This document consists of 28 pages
[redacted] copies,

LOS ALAMOS SCIENTIFIC LABORATORY
OF THE UNIVERSITY OF CALIFORNIA LOS ALAMOS NEW MEXICO

REPORT WRITTEN: July 1956

REPORT DISTRIBUTED: NOV 27 1956

SCATTERING OF FAST NEUTRONS BY U^{238}

Work done by:

J. R. Beyster
M. Walt
R. G. Schrandt

Report written by:

M. Walt
J. R. Beyster

Contract W-7405-ENG. 36 with the U. S. Atomic Energy Commission

[redacted]

[redacted] UNCLASSIFIED

PHYSICS AND MATHEMATICS
LA-2061

Los Alamos Report Library	1-20
AF Plant Representative, Burbank	21
AF Plant Representative, Marietta	22
AF Plant Representative, Seattle	23-24
AF Plant Representative, Wood-Ridge	25
ANP Project Office, Fort Worth	26
Alco Products, Inc.	27
Argonne National Laboratory	28-31
Armed Forces Special Weapons Project, Sandia	32
Armed Forces Special Weapons Project, Washington	33
Army Chemical Center	34
Atomic Energy Commission, Washington	35-37
Battelle Memorial Institute	38
Bettis Plant (WAPD)	39-42
Brookhaven National Laboratory	43-45
Bureau of Ships	46
Chicago Patent Group	47
Chief of Naval Research	48
Columbia University (Havens)	49
Combustion Engineering, Inc. (CERD)	50
Convair-General Dynamics Corporation	51
Dow Chemical Company (Rocky Flats)	52
duPont Company, Aiken	53-55
Engineer Research and Development Laboratories	56
Foster Wheeler Corporation	57
General Electric Company (ANPD)	58-61
General Electric Company, Richland	62-69
Goodyear Atomic Corporation	70-71
Hanford Operations Office	72
Headquarters, Air Force Special Weapons Center	73
Iowa State College	74
Knolls Atomic Power Laboratory	75-78
Massachusetts Institute of Technology (Ashby)	79
Mound Laboratory	80
National Advisory Committee for Aeronautics, Cleveland	81
National Bureau of Standards	82
Naval Air Development and Material Center	83
Naval Medical Research Institute	84
Naval Research Laboratory	85-86
New Brunswick Area Office	87
New York Operations Office	88-89
New York University	90
North American Aviation, Inc.	91-93
Nuclear Development Corporation of America	94
Nuclear Metals, Inc.	95
Office of the Chief of Naval Operations (OP-361)	96
Patent Branch, Washington	97
Phillips Petroleum Company (NRTS)	98-101
Pratt & Whitney Aircraft Division (Fox Project)	102
Sandia Corporation	103
Special Devices Center	104
Sylvania Electric Products, Inc.	105
Union Carbide Nuclear Company (C-31 Plant)	106
Union Carbide Nuclear Company (K-25 Plant)	107-108
Union Carbide Nuclear Company (ORNL)	109-114
USAF Project RAND	115
U. S. Naval Postgraduate School	116
U. S. Naval Radiological Defense Laboratory	117
UCLA Medical Research Laboratory	118
University of California Radiation Laboratory, Berkeley	119-120
University of California Radiation Laboratory, Livermore	121-123
University of Rochester	124
Vitro Engineering Division	125
Wright Air Development Center (WCOSI-3)	126-131
Yale University	132
Glenn L. Martin Company	133
Richard G. Rowe	134
Technical Information Service Extension (For Official AEC Use)	135-149
Technical Information Service Extension	150-199
Special Distribution:	
Manager, ALO (Russell Ball)	200

ABSTRACT

Differential cross sections for elastic scattering at 2.5, 4.1, and 7.0 Mev neutron energies and non-elastic cross sections at 2.5 and 7.0 Mev neutron energies have been measured for U^{238}. These data and other experimental information for U^{238} have been utilized in the selection of parameters for a complex potential well representation of the nucleus. This nuclear model has then been used to calculate nuclear penetrabilities and elastic scattering, compound nucleus formation, and transport cross sections at neutron energies from 25 kev to 18 Mev.

APPROVED FOR PUBLIC RELEASE

1. INTRODUCTION

Cross sections for the interaction of fast neutrons with uranium are of considerable value in calculating the behavior of multiplying assemblies. Of particular interest are the differential cross section for elastic scattering and the non-elastic cross section, which is defined as the total cross section minus the elastic cross section. For fissionable elements, therefore, the non-elastic or inelastic collision cross section is the sum of the cross sections for all capture, fission, and inelastic scattering processes, including such reactions as (n,γ), (n, fission), and (n,n'). The purpose of this report is to present, in a convenient form for reactivity and shielding calculations, the available data on the angular distributions of neutrons scattered by uranium and on the non-elastic cross sections.

The measurements of these cross sections for uranium were performed in conjunction with a series of experiments on a number of non-fissionable elements. The experiments with the non-fissionable elements are described in Refs. 1 and 2; however, the uranium work has not been published previously. In Section 4 of this paper the available data are interpreted in terms of a complex potential well[3] and the parameters of the well are adjusted to give agreement with experiment. Calculations with these chosen parameters are also made at intermediate energies to obtain "interpolated" values of the cross sections at energies where experimental values do not exist.

2. DIFFERENTIAL CROSS SECTION FOR ELASTIC SCATTERING

The experimental values of the differential cross section for elastic scattering of neutrons by uranium are indicated by the circles in Figs. 6, 8, 11, 12, 13, and 17. The experimental techniques used to obtain these results are described in Refs. 1, 2, and 4.

The analysis of the data for fissionable elements differs from that for non-fissionable elements only in requiring a correction for the fission neutrons produced in the scattering sample. This correction is negligible

at 1 Mev, where the fission cross section is small, and at 7 Mev, where only a small amount of the fission spectrum lies above the detection threshold of the counter. At the intermediate energies of 2.5 to 4 Mev, where the effects of fission neutrons are appreciable, corrections were made by two independent methods.

In the first method, the apparent increase in the observed differential cross section for elastic scattering caused by the presence of fission spectrum neutrons was computed by the expression

$$\frac{\sigma_f \nu}{4\pi} \int_0^\infty S(E)\ N(E)\ dE$$

where σ_f is the fission cross section, ν the average number of neutrons emitted per fission, S(E) the energy sensitivity of the neutron detector, and N(E) dE the flux of neutrons between energy E and energy E + dE in the fission spectrum. The angular distribution of fission neutrons was assumed to be isotropic to a first approximation at 2.5, 4.1, and 7.0 Mev in agreement with the experiments of Brolley et al.[5] and J. S. Fraser[6] and with measurements of this distribution at 0.5 and 1.0 Mev[7] and 3.0 Mev.[8]

The second method of correcting for fission neutrons was suggested by H. H. Barschall and is described as follows. If the bombarding neutrons are of energy E_0 and the counter used to measure the scattered neutrons has a detection threshold at A, where $A < E_0$, the threshold of a second counter is set at B, where $B > E_0$. The counts at threshold B are due to high-energy fission neutrons and the number of counts C(B) obtained in counter B during a run is proportional to the number of fissions occurring in the scattering sample. If the incident energy is lowered below A, the ratio of fission counts C'(A) in counter A to the fission counts C'(B) in counter B can be obtained. The number of fission counts recorded by counter A during a run in which elastic scattering is measured is then

$$\frac{C'(A)}{C'(B)}\ C(B)$$

Both of these correction methods require the assumption that the fission neutron spectrum does not change appreciably with incident neutron energy. However, the second method does not require a knowledge of the fission cross section, the average number of neutrons released per fission, or the angular distribution of fission neutrons. The corrections obtained by the two methods were in good agreement.

3. NON-ELASTIC (INELASTIC COLLISION) CROSS SECTIONS

Non-elastic cross sections for uranium were obtained by two methods: (1) by subtracting measured elastic cross sections from total cross sections and (2) by the sphere transmission technique. The first method is discussed for non-fissionable elements in Refs. 1 and 4, and the methods of correcting for fission in the scattering sample are given in Section 2 of this report. The second method for determining non-elastic cross section, the sphere transmission technique, is discussed in Reference 2. These measurements also had to be corrected for the sensitivity of the detector to fission neutrons originating in the uranium spheres. The methods of making this correction are equivalent to those given in Section 2 of this report and are also discussed in LA-1939.[9] The cross sections obtained by the two methods are in good agreement.

The available data on the non-elastic cross section of U^{238} are indicated by the triangles in Fig. 1. The solid curve that passes through most of the experimental points is a calculated curve of the cross section for compound nucleus formation and is discussed in Section 4. The cross sections measured at 2.5 and 7.0 Mev neutron energies have not been reported previously. The remainder of the experimental information is given in Refs. 7 and 9.

4. OPTICAL MODEL CALCULATIONS

Recent calculations[2] have shown that rather accurate values of the total cross section, the differential elastic scattering cross section, and the non-elastic cross section can be obtained from an optical model potential that contains parameters evaluated by comparison of theory and experiment. This ability of the theory to reproduce experimental data suggests a means of obtaining reasonable estimates of these cross sections at energies where experimental information is not available. If the adjustable parameters of the theory are chosen so that the calculated cross sections agree with existing measurements, then calculations with these same parameters should provide an excellent method of interpolating between existing data and extrapolating to energies where experiments have not been performed.

The radial variation of the nuclear potential used in these calculations is given by

$$V(r) = \frac{V_o(1 + i\zeta)}{1 + \exp\left(\frac{r - R}{a}\right)} \qquad (1)$$

where V_o is the well depth, ζ is the absorption parameter, R is the nuclear radius, and a is the diffuseness parameter.

The values of the parameters given in Table I were adjusted to fit the experimental differential elastic cross section at 0.5, 1.0, 2.5, 4.1, 7, and 14 Mev, and the total cross section and non-elastic cross section as functions of energy. The measurements on total differential scattering cross sections for U^{238} (Langsdorf et al.[10]) were also considered in assigning the parameters at neutron energies below 1.0 Mev. Although R and a are constant with energy, V_o and ζ are somewhat energy dependent. The Table I parameters are similar to those that give a good description of the scattering of fast neutrons by bismuth.

The total neutron cross sections computed with the Table I parameters are shown in Fig. 1. The experimental points of Henkel et al.[11] are also shown. The calculated cross sections agree to within 10 percent with the experimental data over the entire energy range.

The differential cross sections for shape-elastic scattering that were calculated by using the potential of Eq. 1 are indicated by the solid and dashed curves in Figs. 2 through 17. Experimental cross sections shown at various neutron energies are the sum of the shape-elastic scattering and compound-elastic scattering cross sections. The dash-dot curves shown in Figs. 2 through 10 were obtained by adding an estimate of the compound-elastic scattering cross section to the calculated shape-elastic cross section. The differential cross section for compound-elastic scattering was assumed to be $1/4\pi$ times the difference between the calculated cross section for compound nucleus formation and the observed non-elastic cross section. When only a solid or dashed curve is shown, the effect of compound-elastic scattering is negligible. The total elastic scattering cross sections obtained by integrating calculated differential elastic scattering cross sections agree to within 10 percent with experimental results.

Although reasonable agreement between theory and the experimental data has been attained, the valleys in the angular distributions are not fit very well by the calculations. This effect has been observed for other elements and may possibly be caused by the neglect of spin-orbit forces and nuclear deformations in this model.

Calculated cross sections for compound nucleus formation, σ_c, are shown by a solid curve in Fig. 1. The experimental non-elastic cross

TABLE I

PARAMETERS FOR OPTICAL MODEL POTENTIAL AND THE CALCULATED PENETRABILITIES FOR U^{238}

E_n (Mev)	$10^{13}R$	V (Mev)	ζ	$10^{13}a$	T_0	T_1	T_2	T_3	T_4	T_5	ℓ_{max}
0.025	8.05	44	0.05	0.5	0.078	0.012	0.0	0.0	0.0	0.0	2
0.05	8.05	44	0.05	0.5	0.11	0.03	0.0	0.0	0.0	0.0	3
0.10	8.05	44	0.05	0.5	0.15	0.08	0.002	0.0	0.0	0.0	3
0.25	8.05	44	0.05	0.5	0.22	0.24	0.015	0.001	0.0	0.0	4
0.50	8.05	44	0.05	0.5	0.28	0.48	0.054	0.015	0.0	0.0	4
0.75	8.05	44	0.062	0.5	0.37	0.65	0.12	0.06	0.0	0.0	4
1.0	8.05	44	0.075	0.5	0.46	0.77	0.20	0.16	0.003	0.0	5
1.5	8.05	44	0.075	0.5	0.50	0.89	0.30	0.46	0.015	0.006	6
2.0	8.05	44	0.075	0.5	0.54	0.95	0.38	0.73	0.04	0.021	6
2.5	8.05	44	0.075	0.5	0.56	0.98	0.43	0.86	0.09	0.05	6
3.0	8.05	43.7	0.075	0.5	0.59	0.98	0.48	0.92	0.14	0.09	7
4.1	8.05	43	0.075	0.5	0.62	0.97	0.54	0.94	0.29	0.21	7
5.0	8.05	43	0.083	0.5	0.68	0.97	0.63	0.90	0.46	0.29	8
6.0	8.05	43	0.091	0.5	0.73	0.96	0.70	0.87	0.63	0.37	9
7.0	8.05	43	0.1	0.5	0.78	0.95	0.77	0.86	0.78	0.45	9
8.0	8.05	43	0.1	0.5	0.81	0.93	0.81	0.83	0.87	0.51	10
9.0	8.05	43	0.1	0.5	0.83	0.91	0.84	0.82	0.92	0.55	10
10.0	8.05	42.5	0.1	0.5	0.84	0.89	0.85	0.81	0.93	0.60	10
11.0	8.05	42.5	0.1	0.5	0.85	0.87	0.87	0.80	0.95	0.64	11
12.0	8.05	42	0.1	0.5	0.86	0.86	0.88	0.80	0.95	0.67	11
13.0	8.05	42	0.1	0.5	0.87	0.85	0.89	0.79	0.94	0.70	11
14.0	8.05	42	0.1	0.5	0.88	0.84	0.90	0.79	0.93	0.73	11
18.0	8.05	42	0.1	0.5	0.89	0.82	0.89	0.79	0.87	0.83	12

sections are shown by triangles. At energies below 2.5 Mev the compound nucleus cross section exceeds the non-elastic cross section because an appreciable fraction of the compound nucleus decay proceeds by the entrance channel (compound-elastic scattering). Between 7 and 14 Mev neutron energies, where no experimental data exist, the non-elastic cross section is assumed to equal the calculated cross section for compound nucleus formation. A slightly better estimate of this quantity than the solid curve is given by the dashed curve. For this estimate the ratio of the compound nucleus to the total cross section is calculated using the optical model, and this ratio is multiplied by the experimental total cross section. This curve of compound nucleus formation cross section can be used to a good approximation for other heavy fissionable nuclei, such as U^{233}, U^{235}, and Pu^{239}. A realistic upper limit on the inelastic scattering cross sections of these elements can then be found by subtracting the fission and capture cross sections from the curve of σ_c.

The experimental transport cross sections shown in Fig. 1 are defined by

$$\sigma_{tr} = \int_0^{\pi} \sigma_{el}(\theta)\ (1-\cos\ \theta)\ d\Omega + \sigma_{ne} \qquad (2)$$

where $\sigma_{el}(\theta)$ is the measured differential cross section for elastic scattering (shape-elastic plus compound-elastic scattering) and σ_{ne} is the measured non-elastic (inelastic collision) cross section. The curve of transport cross section in Fig. 1 is obtained from the optical model calculations by the formula

$$\sigma_{tr} = \int_0^{\pi} \sigma_{se}(\theta)\ (1-\cos\ \theta)\ d\Omega + \sigma_c \qquad (3)$$

where $\sigma_{se}(\theta)$ is the differential cross section for shape-elastic scattering and σ_c is the cross section for compound nucleus formation.

These two methods of defining the transport cross section give identical results regardless of how much compound-elastic scattering occurs. The only requirement is that compound-elastic scattering be symmetrical around 90 degrees. The calculated values shown by the solid curve are in reasonable agreement with experiment.

For many applications it is important to know what fraction of the compound nucleus formation cross section is due to a particular partial wave. For this purpose transmission coefficients or penetrabilities $T_\ell(E)$

were determined routinely during the course of the optical model calculations. T_ℓ (E) is related to σ_c^ℓ, the cross section for compound nucleus formation due to a partial wave of angular momentum ℓ, by

$$\sigma_c^\ell = (2\ell + 1)\ \pi\ T_\ell(E)$$

The T_ℓ (E) values for $\ell \leq 5$ are listed in Table I. The maximum ℓ used in the calculations of the total, compound, and differential elastic scattering cross sections is also given.

REFERENCES

1. M. Walt and J. R. Beyster, Phys. Rev. 98, 677 (1955); Beyster, Henkel, Nobles, and Kister, Phys. Rev. 98, 1216 (1955).
2. J. R. Beyster and M. Walt, Phys. Rev. (to be published).
3. R. D. Woods and D. S. Saxon, Phys. Rev. 95, 577 (1954); Milkanoff, Moszkowski, Nodvik, and Saxon, Phys. Rev. 101, 507 (1956).
4. M. Walt and H. H. Barschall, Phys. Rev. 93, 1062 (1954).
5. Brolley, Dickinson, and Henkel, Phys. Rev. 99, 159 (1955).
6. J. S. Fraser, Phys. Rev. 88, 536 (1952).
7. Allen, Walton, Perkins, Olson, and Taschek, Phys. Rev. (to be published).
8. M. Walt and J. R. Beyster, unpublished data.
9. Bethe, Beyster, and Carter, Los Alamos Scientific Laboratory Report LA-1939, August 1955.
10. Langsdorf, Lane, and Monahan, Argonne National Laboratory Report ANL-5567, June 1956.
11. Henkel, Cranberg, Jarvis, Nobles, and Perry, Phys. Rev. 94, 141 (1954).
12. J. H. Coon, private communication.

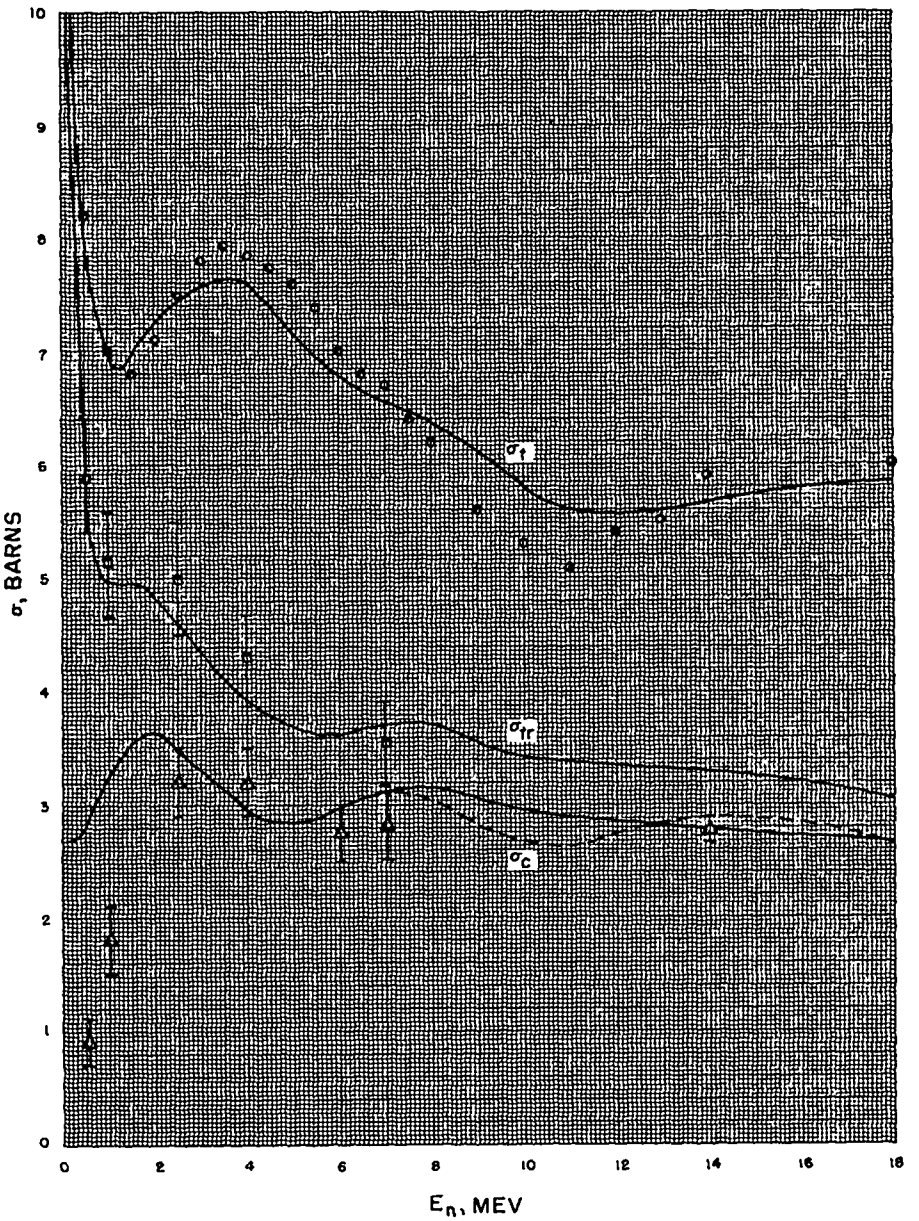

Fig. 1 Cross sections for U^{238}. Circles are measured total neutron cross sections; the curve was calculated using the parameters of Table I. Squares are measured transport cross sections; the curve is calculated. Triangles are measured non-elastic cross sections; the solid curve is the calculated cross section for compound nucleus formation. The dashed curve, based on measured values of the total cross section, is a better estimate of the non-elastic cross section.

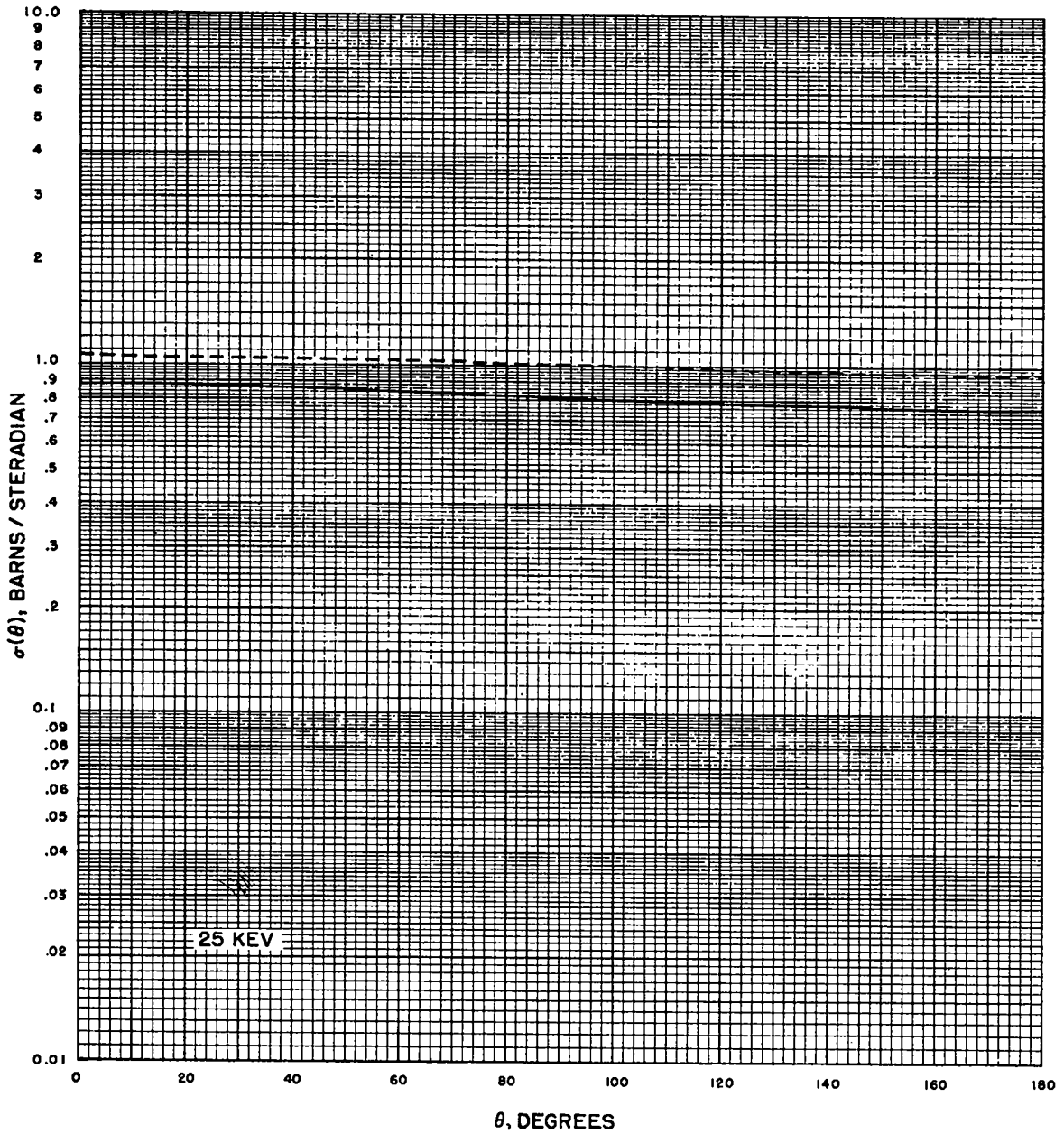

Fig. 2 Differential cross sections at 25 kev. The solid curve is the calculated shape-elastic scattering cross section; the dash-dot curve is the shape-elastic plus an estimate of the compound-elastic cross section.

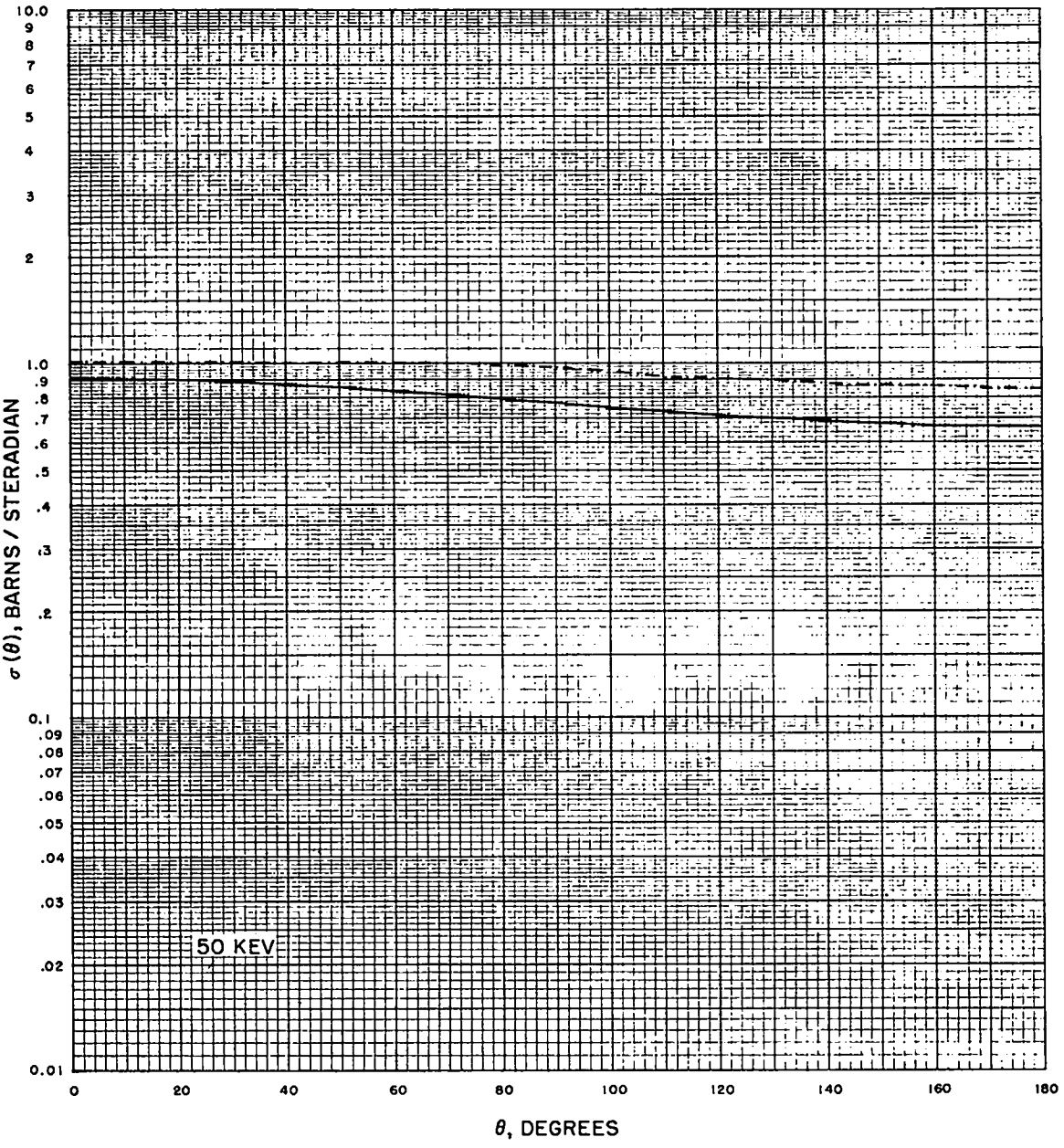

Fig. 3 Differential cross sections at 50 kev. The solid curve is the calculated shape-elastic scattering cross section; the dash-dot curve is the shape-elastic plus an estimate of the compound-elastic cross section.

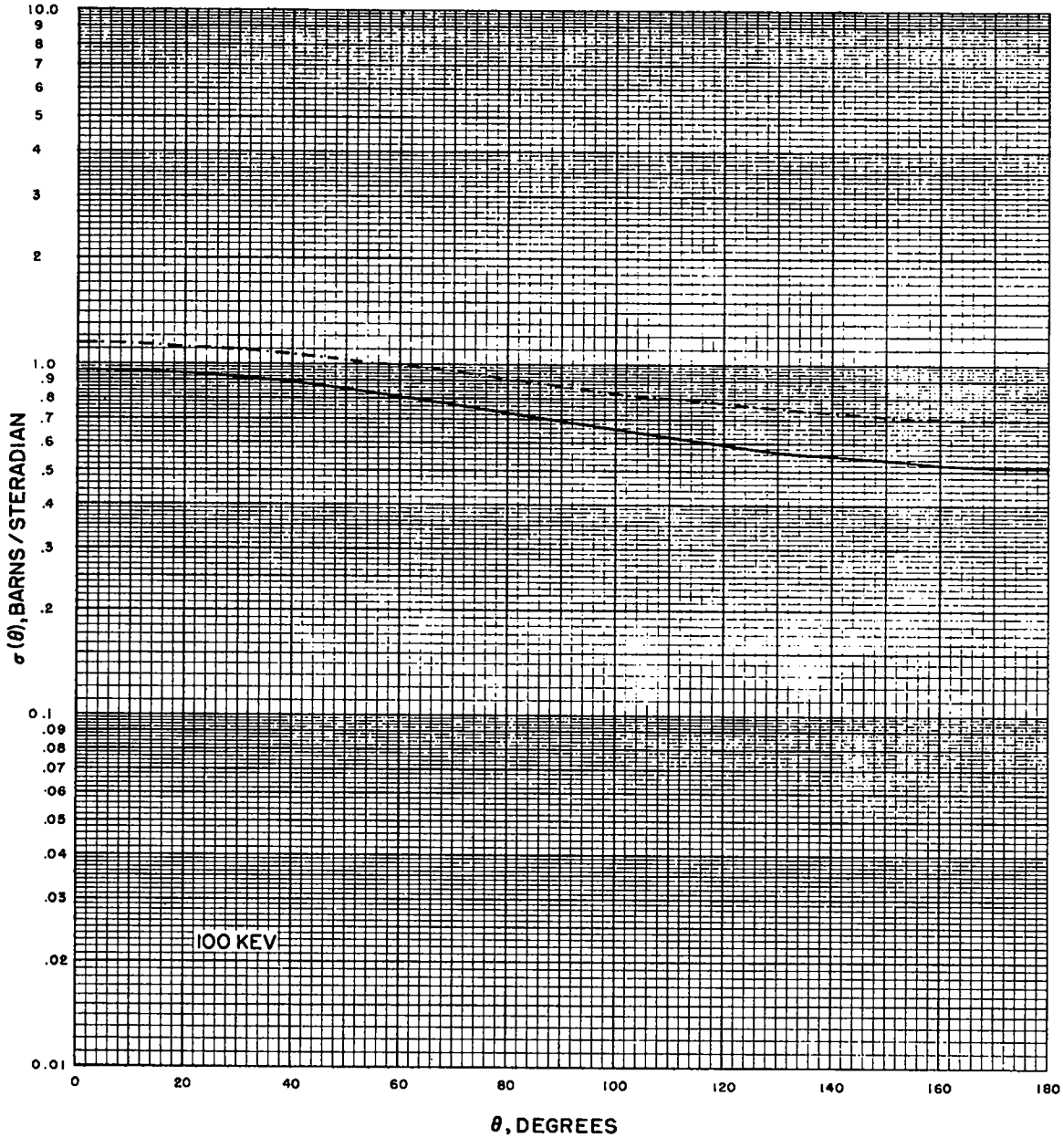

Fig. 4 Differential cross sections at 100 kev. The solid curve is the calculated shape-elastic scattering cross section; the dash-dot curve is the shape-elastic plus an estimate of the compound-elastic cross section.

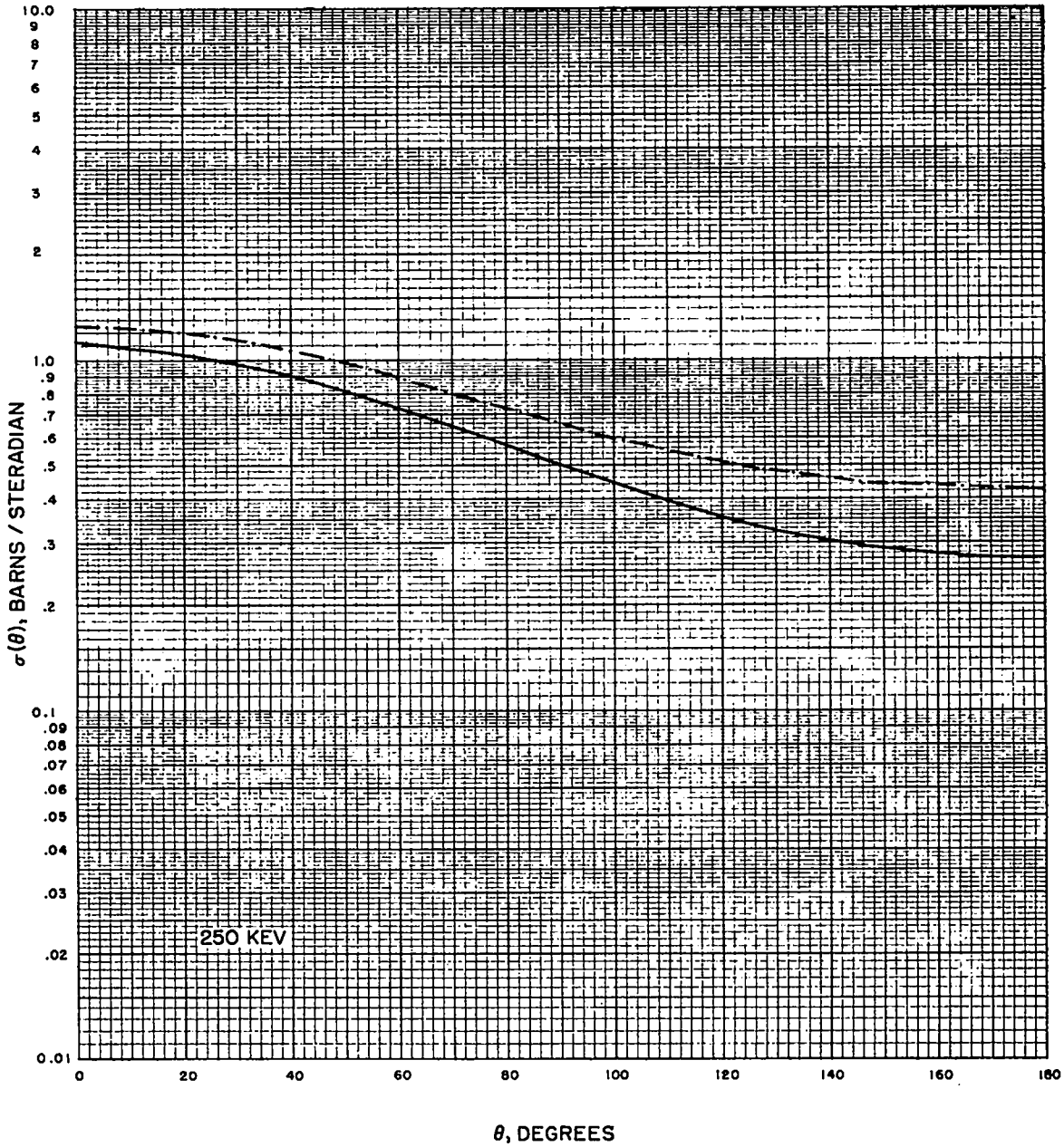

Fig. 5 Differential cross sections at 250 kev. The solid curve is the calculated shape-elastic scattering cross section; the dash-dot curve is the shape-elastic plus an estimate of the compound-elastic cross section.

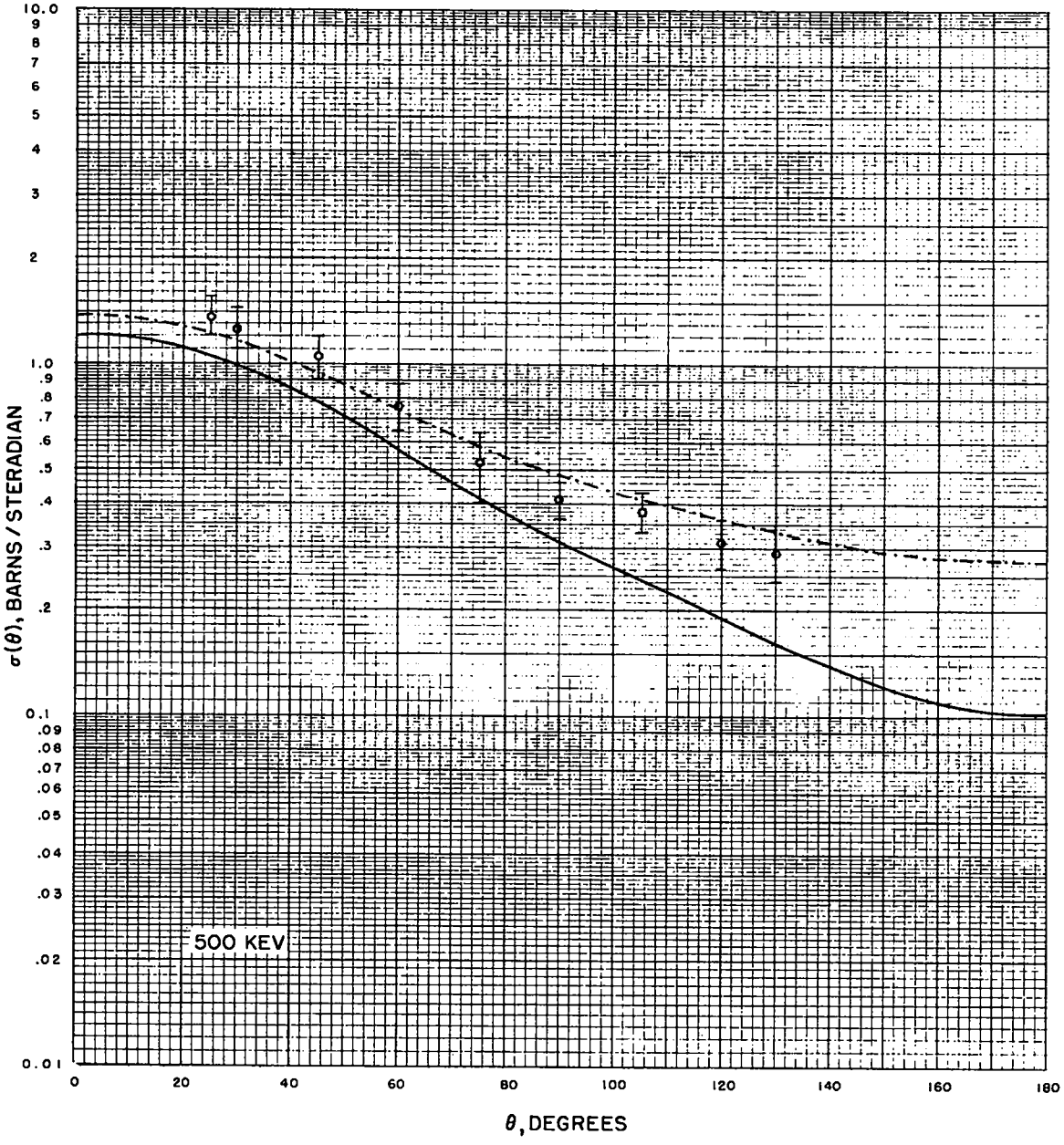

Fig. 6 Differential cross sections at 500 kev. Experimental values are from Ref. 7. The solid curve is the calculated shape-elastic scattering cross section; the dash-dot curve is the shape-elastic plus an estimate of the compound-elastic cross section.

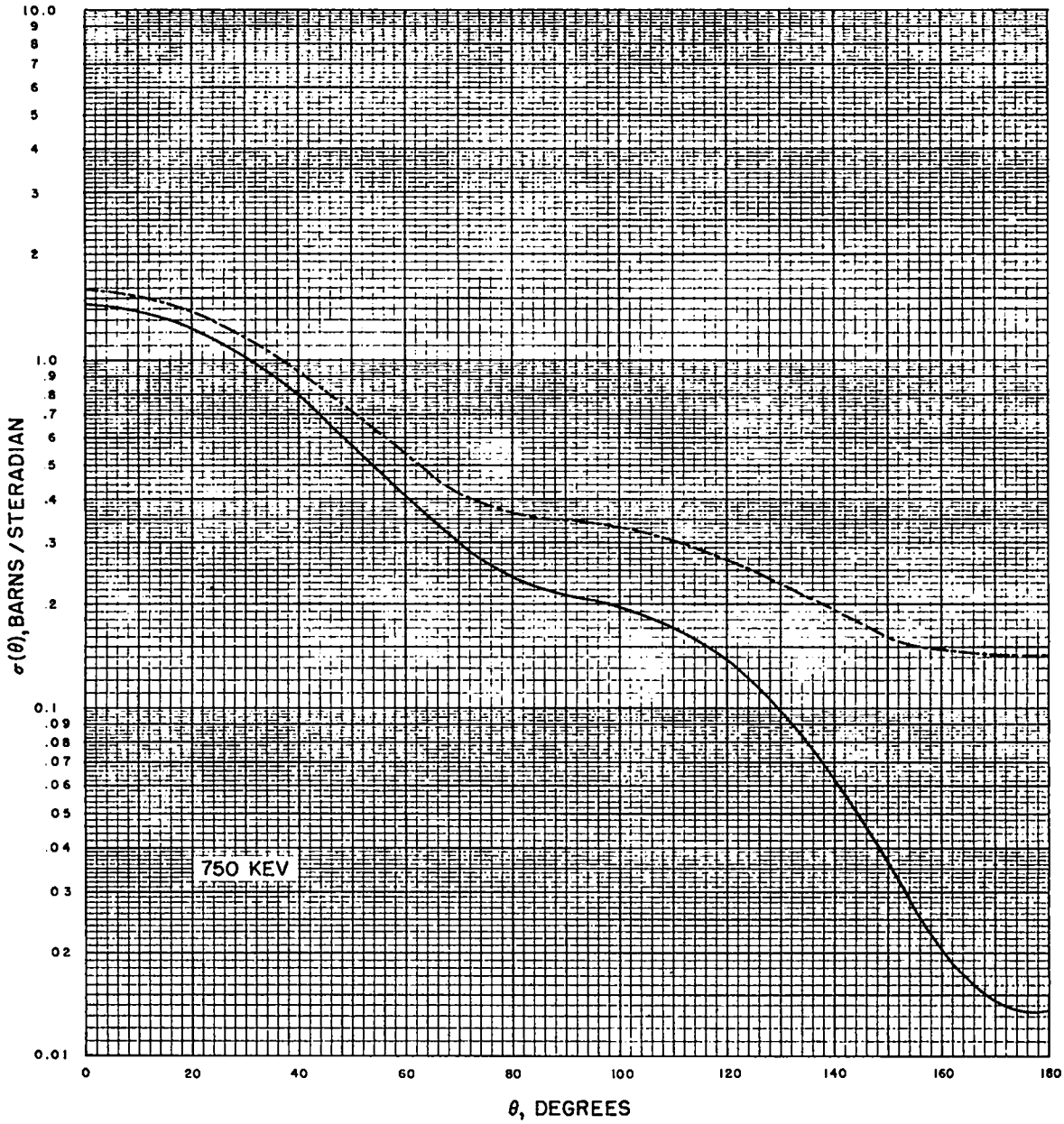

Fig. 7 Differential cross sections at 750 kev. The solid curve is the calculated shape-elastic scattering cross section; the dash-dot curve is the shape-elastic plus an estimate of the compound-elastic cross section.

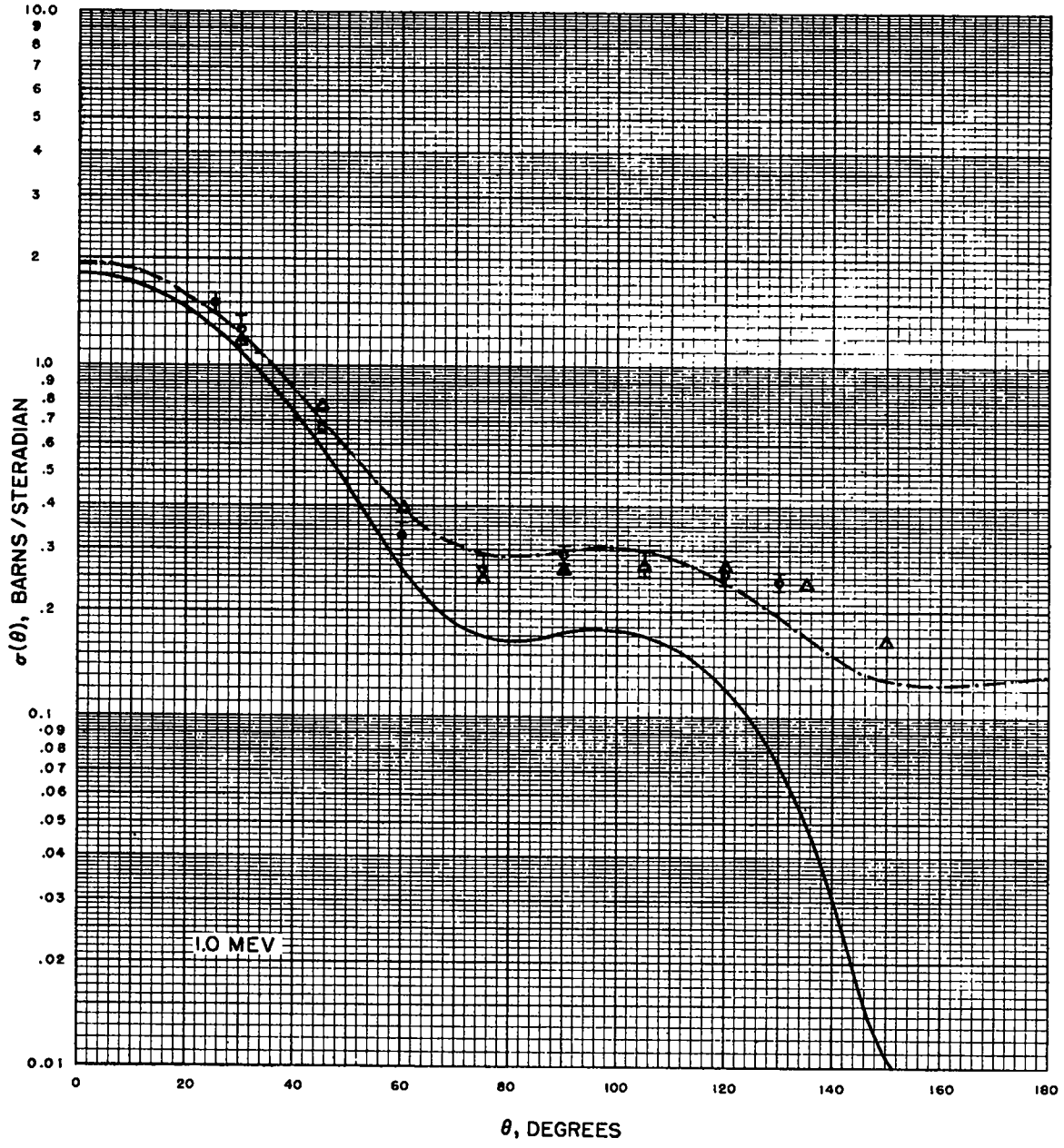

Fig. 8 Differential cross sections at 1.0 Mev. Experimental values are from Refs. 4 and 7. The solid curve is the calculated shape-elastic scattering cross section; the dash-dot curve is the shape-elastic plus an estimate of the compound-elastic cross section.

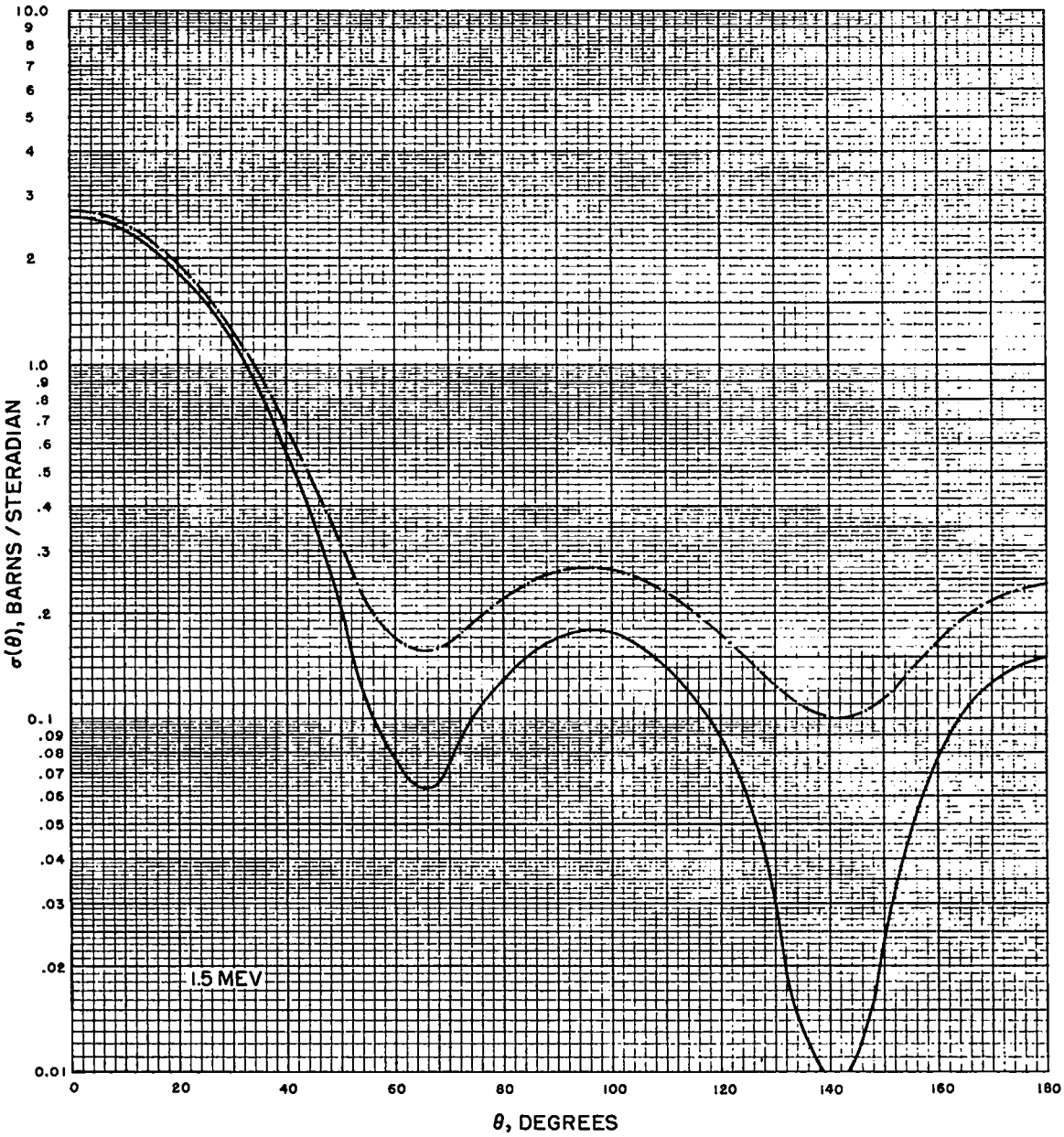

Fig. 9 Differential cross sections at 1.5 Mev. The solid curve is the calculated shape-elastic scattering cross section; the dash-dot curve is the shape-elastic plus an estimate of the compound-elastic cross section.

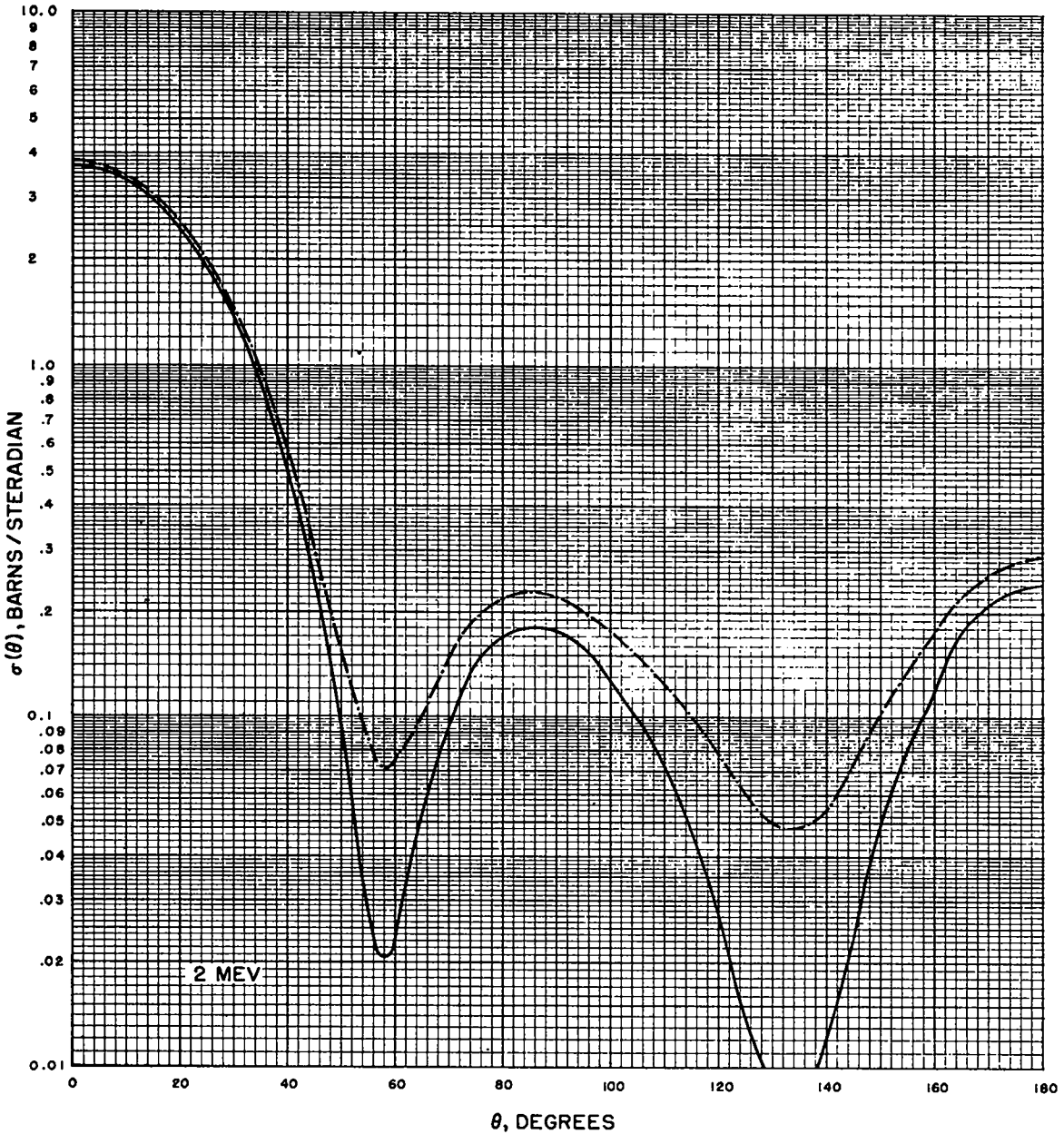

Fig. 10 Differential cross sections at 2.0 Mev. The solid curve is the calculated shape-elastic scattering cross section; the dash-dot curve is the shape-elastic plus an estimate of the compound-elastic cross section.

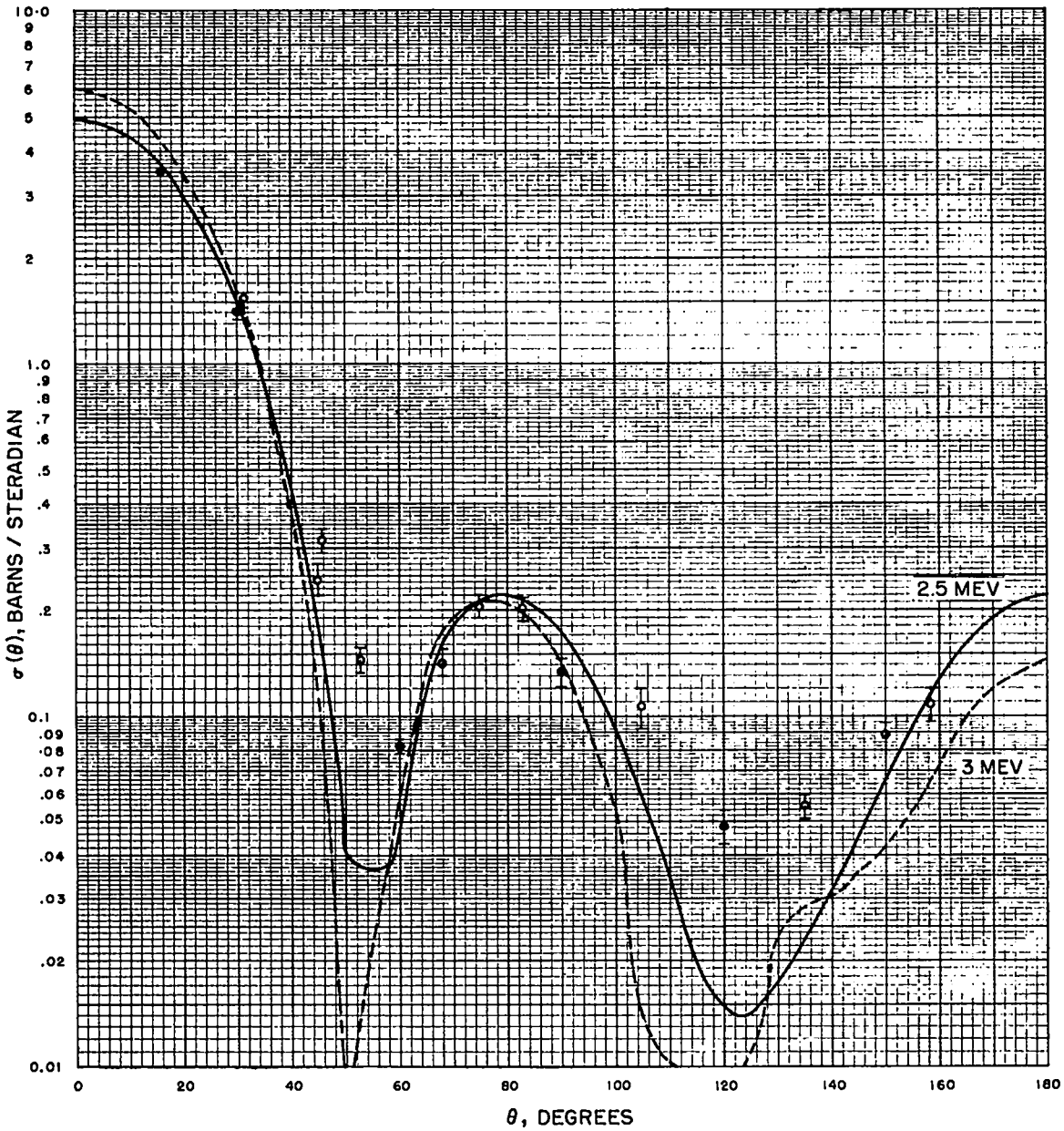

Fig. 11 Experimental values of differential cross section at 2.5 Mev are from the present work. The solid and dashed curves are calculated differential cross sections for elastic scattering.

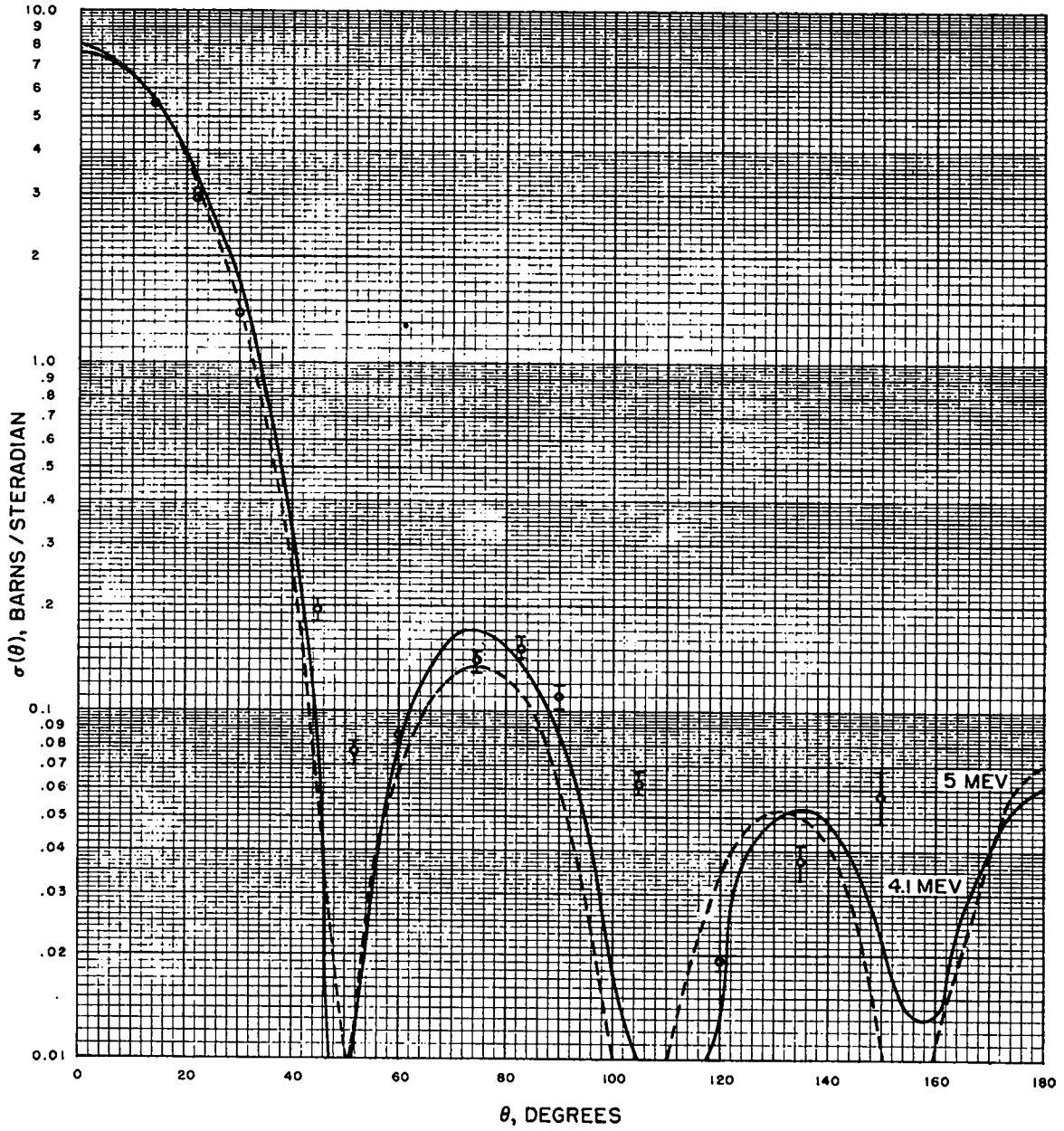

Fig. 12 Experimental values of differential cross section at 4.1 Mev are from the present work. The solid and dashed curves are calculated differential cross sections for elastic scattering.

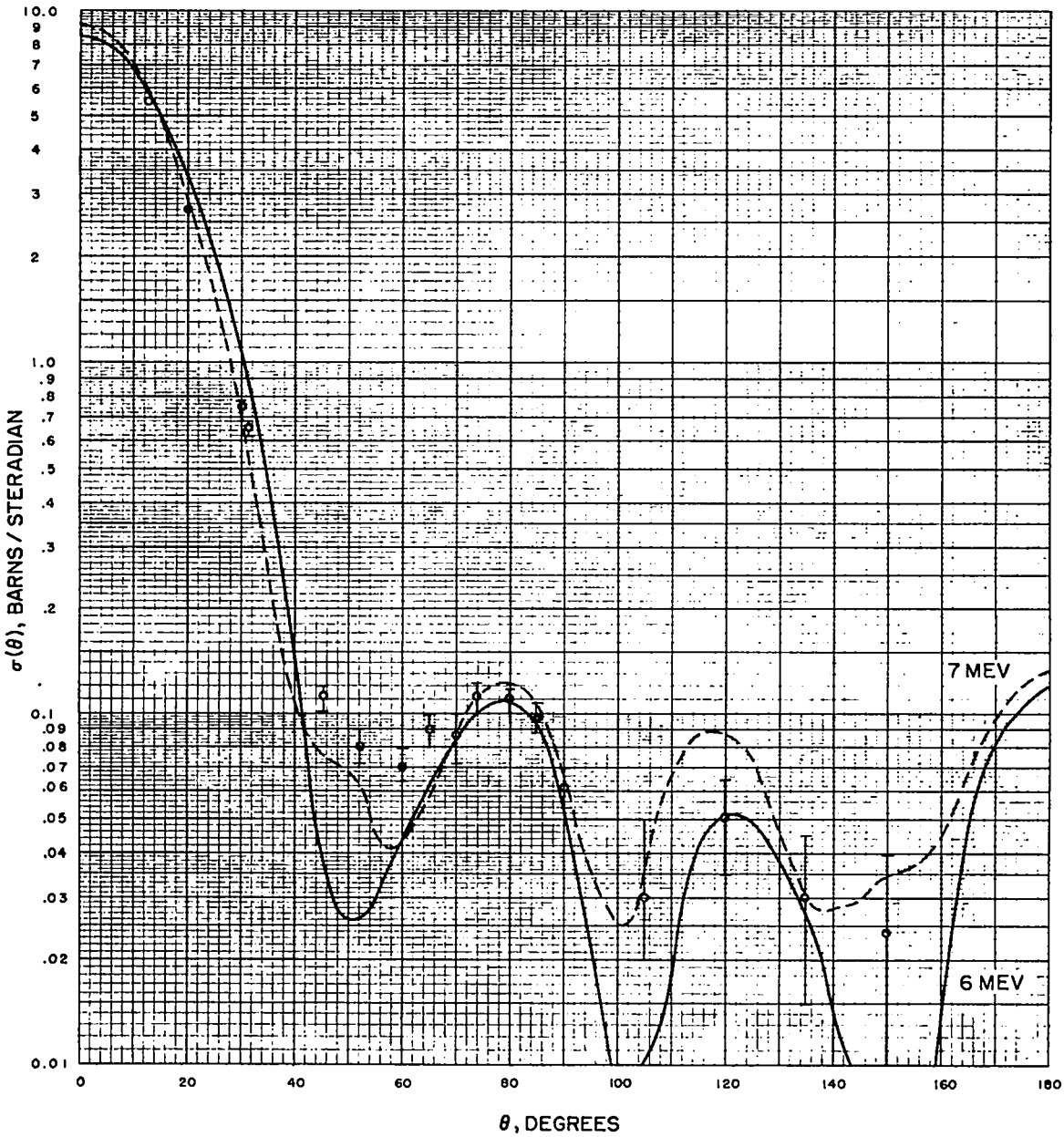

Fig. 13 Experimental values of differential cross section at 7 Mev are from the present work. The solid and dashed curves are calculated differential cross sections for elastic scattering.

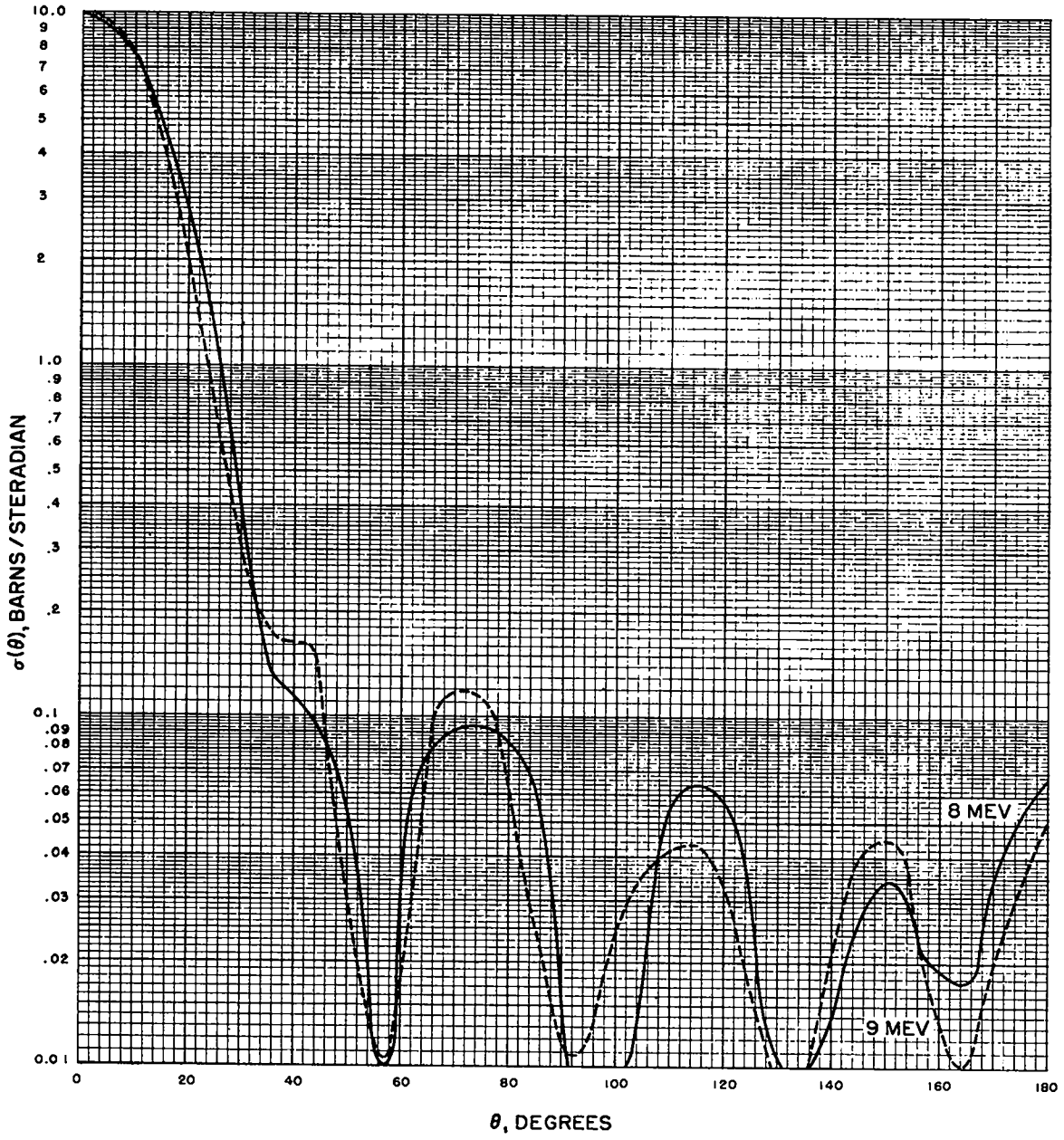

Fig. 14 Calculated differential cross sections for elastic scattering at 8 and 9 Mev.

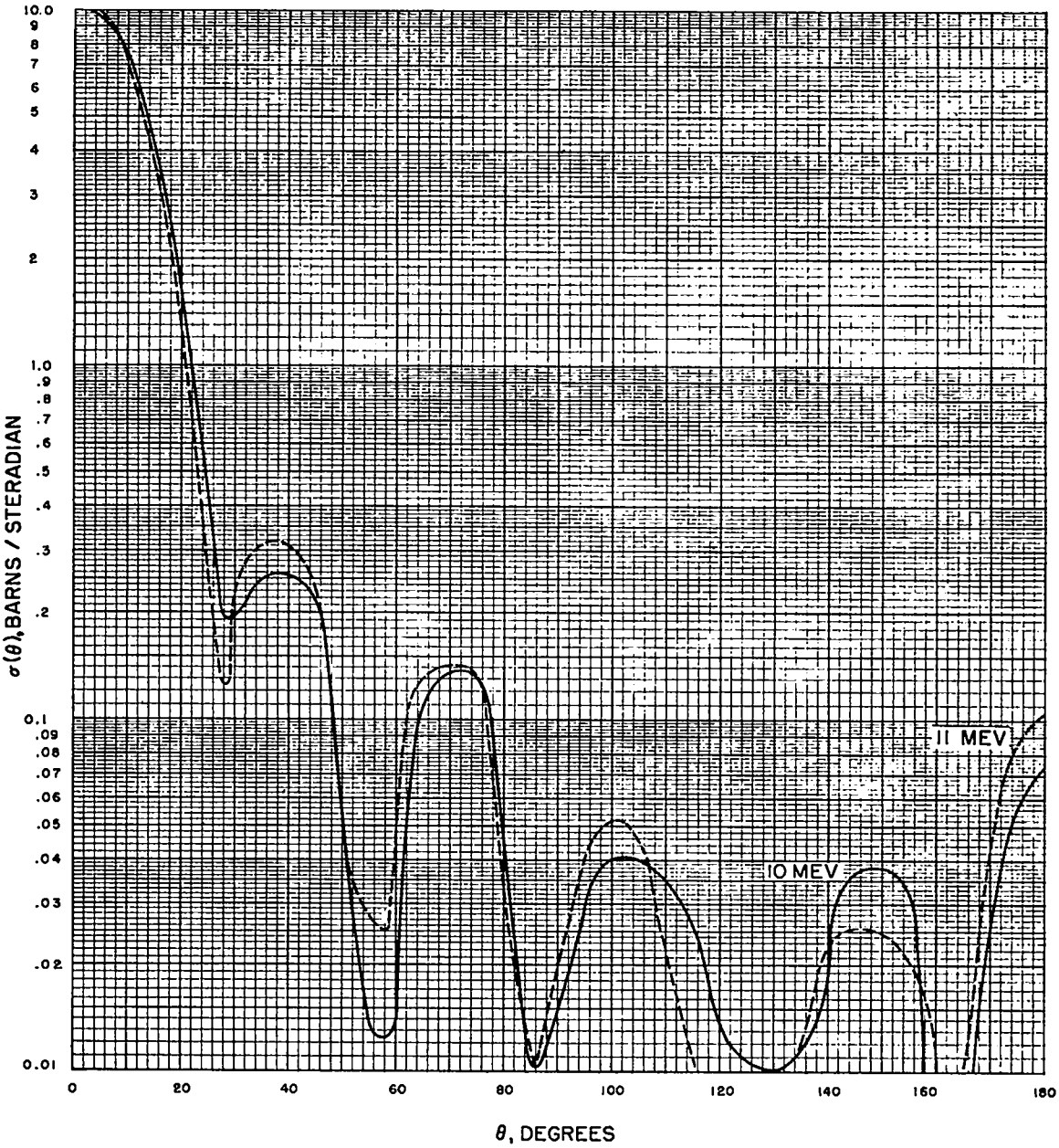

Fig. 15 Calculated differential cross sections for elastic scattering at 10 and 11 Mev.

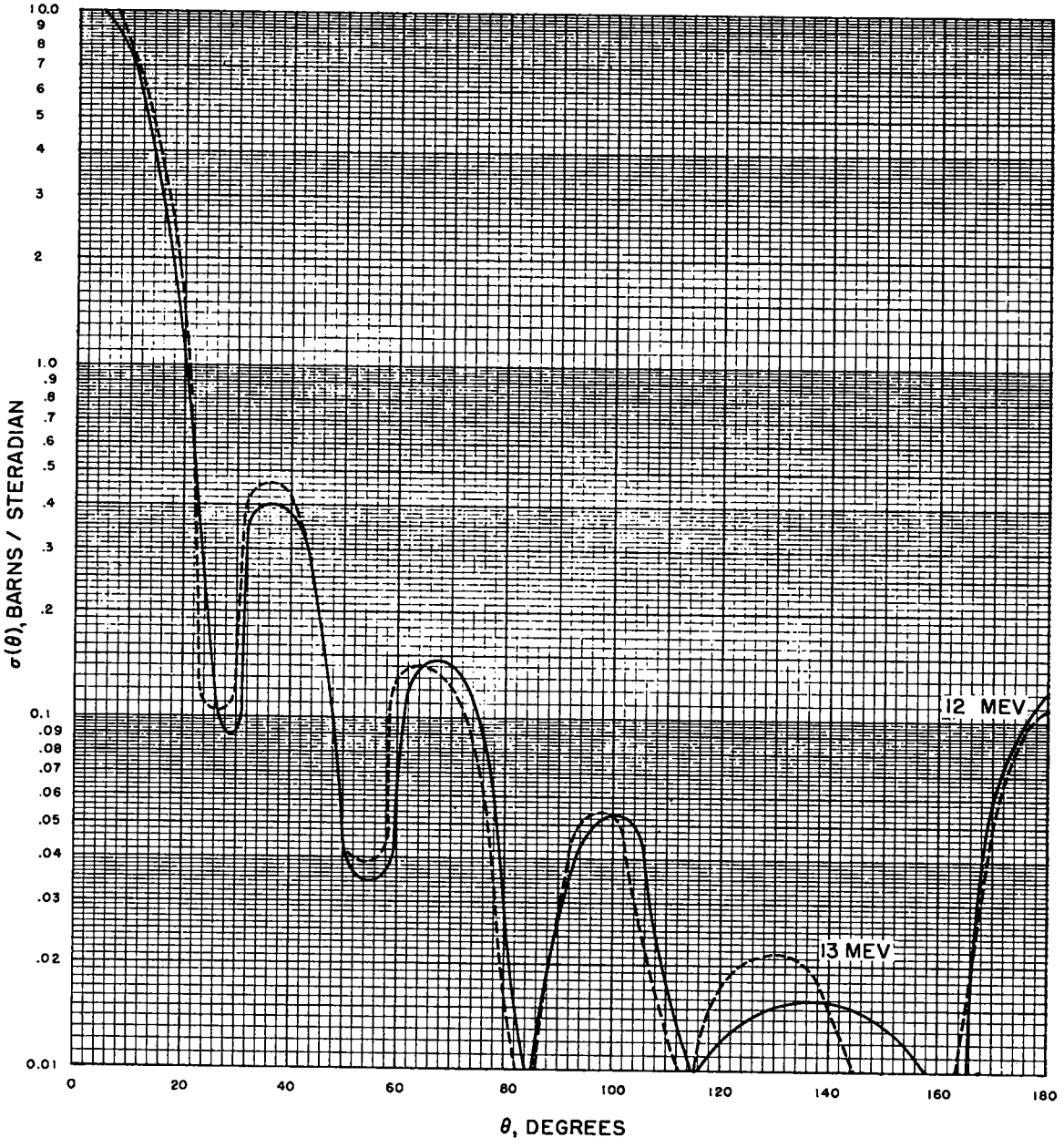

Fig. 16 Calculated differential cross sections for elastic scattering at 12 and 13 Mev.

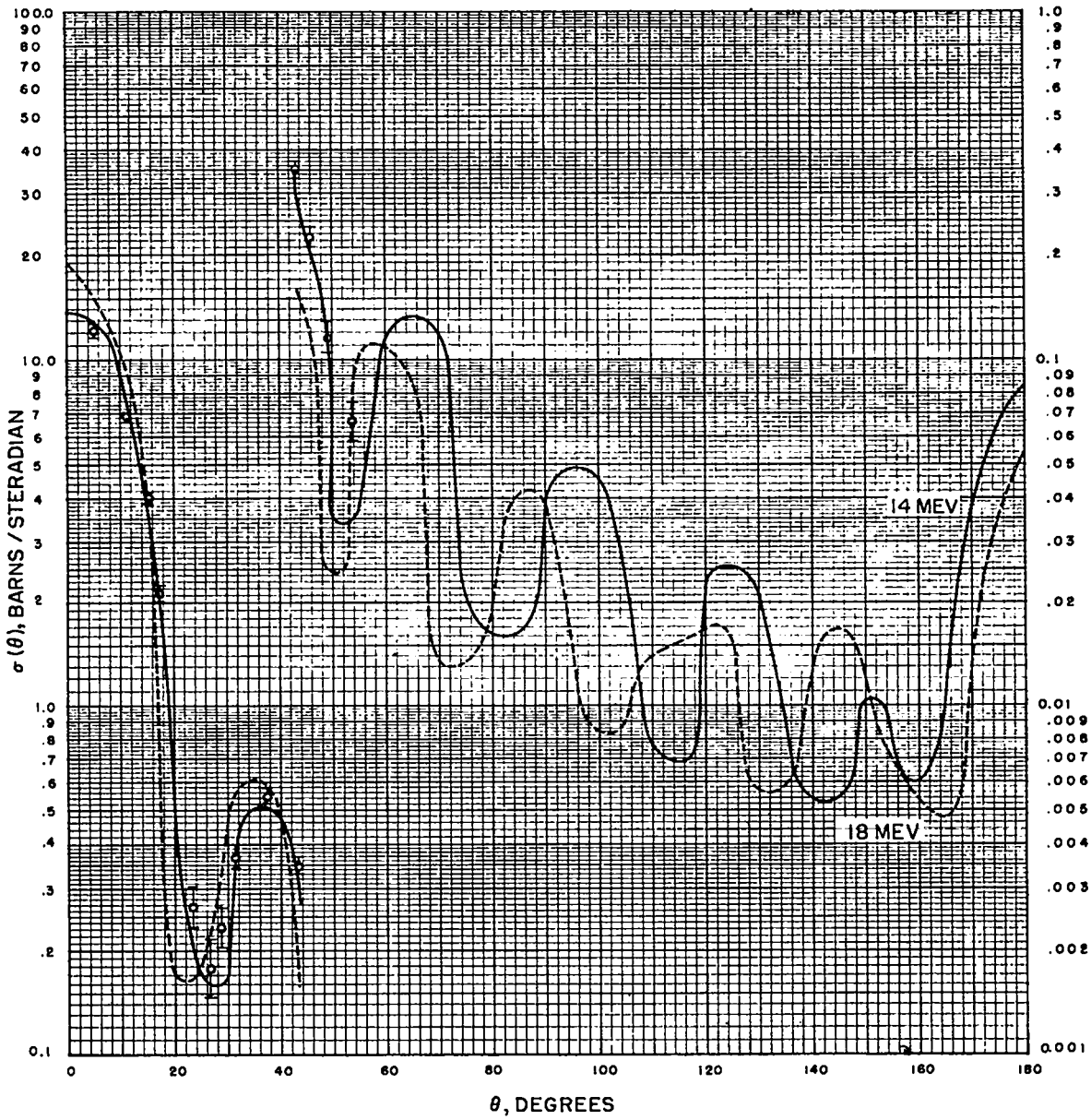

Fig. 17 Experimental values of differential cross section at 14.1 Mev are from Ref. 12. The solid and dashed curves are calculated differential cross sections for elastic scattering. Scale left through 43 degrees, scale right for remainder of curve.